Diurnal variation of ozone depletion during the October–November 2003 solar proton events

Pekka T. Verronen,[1] Annika Seppälä,[1] Mark A. Clilverd,[2] Craig J. Rodger,[3] Erkki Kyrölä,[1] Carl-Fredrik Enell,[4] Thomas Ulich,[4] and Esa Turunen[4]

Received 30 November 2004; revised 16 February 2005; accepted 15 April 2005; published 22 July 2005.

[1] We have studied the short-term effect of the October–November 2003 series of solar proton events on the middle atmosphere. Using the proton flux measurements from the GOES–11 satellite as input, we modeled the effect of the precipitating particles between 26 October and 6 November with a one–dimensional ion and neutral chemistry model. Then we compared the results with ground-based radio propagation measurements, as well as with NO_2 and ozone profiles made by the GOMOS satellite instrument. The very low frequency signal experiences up to −7 dB absorption during the largest solar proton event, subsequently varying with time of day during the recovery phase. The model and radio propagation observations show very good agreement, suggesting that the model is capturing the impact of solar protons on the ionosphere. The model results show order-of-magnitude changes in odd hydrogen and odd nitrogen concentrations, as well as ozone depletion varying from 20% at 40 km altitude to more than 95% at 78 km. The magnitude and altitude distribution of ozone depletion is found to depend not only on the flux and energy of the protons but also on the diurnal cycle of atomic oxygen and ozone-depleting constituents so that the largest depletions of ozone are seen during sunrise and sunset. The after-event recovery of ozone is altitude-dependent because of the differences in the recovery of odd hydrogen and odd nitrogen and also because of a relatively faster ozone production at higher altitudes. The modeled and measured NO_2 profiles agree well at altitudes 35–60 km, particularly during times of large concentrations observed after the solar proton event onset. A comparison of the time series of ozone depletion shows a good agreement between the model and observations.

Citation: Verronen, P. T., A. Seppälä, M. A. Clilverd, C. J. Rodger, E. Kyrölä, C.-F. Enell, T. Ulich, and E. Turunen (2005), Diurnal variation of ozone depletion during the October–November 2003 solar proton events, J. Geophys. Res., 110, A09S32, doi:10.1029/2004JA010932.

1. Introduction

[2] Solar proton events (SPE) correspond to solar coronal mass ejections (CME) during which a large amount of protons and heavier ions are emitted [Reames, 1999], sometimes toward the Earth. Solar protons entering the Earth's magnetosphere are guided by the Earth's magnetic field and precipitate into the polar cap areas [Patterson et al., 2001]. Since the protons can have very high energies, up to tens of MeVs, they deposit their energy in the mesosphere and stratosphere. Thus they provide a direct connection between the Sun and the Earth's middle atmosphere. SPEs are relatively sporadic (only a few large solar proton events with proton energies sufficient to penetrate down to the stratopause region reach Earth during a solar maximum) but are extreme examples of solar forcing on the middle atmosphere.

[3] The precipitating particles produce (1) odd hydrogen HO_x (H + OH + HO_2) through chemistry associated with ion pair production, water cluster ion formation, and subsequent neutralization, and (2) odd nitrogen NO_x (N + NO + NO_2) through dissociation of molecular nitrogen via charged particle impact and ion chemistry [Crutzen et al., 1975; Solomon et al., 1981; Rusch et al., 1981]. HO_x and NO_x play a key role in ozone balance of the middle atmosphere because they destroy odd oxygen through catalytic reactions [see, e.g., Brasseur and Solomon, 1986, pp. 291–299]. The produced HO_x has a relatively short lifetime (few days), but without solar radiation NO_x chemical loss is inefficient in the mesosphere. Thus in conditions of low level of solar illumination it could stay at an elevated level for months after an event. Significant depletion of middle atmospheric ozone after large solar proton events has been predicted by atmospheric modeling [Rusch et al., 1981; Solomon et al., 1983; Reid et al., 1991; Jackman et

[1]Finnish Meteorological Institute, Earth Observation, Helsinki, Finland.
[2]British Antarctic Survey (NERC), Cambridge, UK.
[3]Physics Department, University of Otago, Dunedin, New Zealand.
[4]Sodankylä Geophysical Observatory, Sodankylä, Finland.

Copyright 2005 by the American Geophysical Union.
0148-0227/05/2004JA010932$09.00

al., 1995, 2000] and this phenomenon has also been captured by satellite measurements [Thomas et al., 1983; McPeters and Jackman, 1985; Jackman et al., 2001; Randall et al., 2001; Seppälä et al., 2004].

[4] The Sodankylä Ion Chemistry model (SIC) is a one-dimensional chemical model designed for ionospheric D-region studies. It solves for concentrations of 63 ions and 13 neutral species in the altitude region 20–150 km. The SIC model includes an extensive range of positive and negative ion chemistry so that the effects of ion chemistry on the neutral atmosphere can be modeled without parameterization. During a solar proton or electron precipitation event the model can be used to monitor the day-to-day and also diurnal variation of HO_x

Table 1. Recent Additions and Changes in the Neutral Chemistry Scheme[a]

Number	Reaction	Rate Coefficient	Source
R1	$N(^2D) + O \longrightarrow N + O$	6.90×10^{-13}	Fell et al. [1990]
R2	$O + H_2 \longrightarrow OH + H$	$8.50 \times 10^{-20} \times T^{2.7} \times e^{-3160/T}$	Sander et al. [2003]
R3	$O + H_2O_2 \longrightarrow OH + HO_2$	$1.40 \times 10^{-12} \times e^{-2000/T}$	Sander et al. [2003]
R4	$O + HO_2 \longrightarrow OH + O_2$	$1.50 \times 10^{-11} \times e^{+200/T}$	See caption
R5	$O_3 + H \longrightarrow OH + O_2$	$2.18 \times 10^{-10} \times e^{-670/T}$	See caption
R6	$HO_2 + HO_2 \longrightarrow H_2O_2 + O_2$	$2.30 \times 10^{-13} \times e^{600/T}$	Sander et al. [2003]
R7	$NO_2 + NO_3 + M \longrightarrow N_2O_5$	$2.00 \times 10^{-30} \times (300/T)^{4.4}$	Sander et al. [2003]
R8	$NO_3 + NO_3 \longrightarrow 2NO_2 + O_2$	$8.50 \times 10^{-13} \times e^{-2450/T}$	Sander et al. [2003]
R9	$NO_2 + H \longrightarrow NO + OH$	$4.00 \times 10^{-10} \times e^{-340/T}$	Sander et al. [2003]

[a]The coefficient of R4 is that of Sander et al. [2003] reduced by 50%. The coefficient of R5 is the lower limit given by Sander et al. [2003]. Notation: M is any atmospheric molecule and T is temperature. Units for reaction R7 are $cm^6\ s^{-1}$ and for the other reactions $cm^3\ s^{-1}$.

[1986]. Solar radiation in wavelengths between 1 and 422.5 nm is considered, ionizing N_2, O_2, O, Ar, He, NO, $O_2(^1\Delta_g)$, CO_2, and dissociating N_2, O_2, O_3, H_2O, H_2O_2, NO, NO_2, HNO_3, and N_2O_5. The photoionization/dissociation cross sections as well as branching ratios for different products were gathered from various sources [Ohshio et al., 1966; McEwan and Phillips, 1975; Torr et al., 1979; Shimazaki, 1984; World Meteorological Organization, 1985; Rees, 1989; Fuller-Rowell, 1993; Minschwaner and Siskind, 1993; Siskind et al., 1995; Koppers and Murtagh, 1996; Sander et al., 2003].

[13] The numerous sources of reaction rate coefficients for the ionic reactions are listed in the work of Turunen et al. [1996] along with the additions listed in the work of Verronen et al. [2002]. The negative ion chemistry scheme and the ion-ion recombination coefficient have been recently checked and revised according to and references therein Kazil et al. [2003]. The neutral chemistry includes 59 reactions of the modeled neutral species, for which the rate coefficients have been updated according to Sander et al. [2003]. Most of these reactions are listed in the work of Verronen et al. [2002]. The additions and changes made for this study are presented in Table 1.

[14] The model includes a vertical transport code, described by Chabrillat et al. [2002], which takes into account molecular and eddy diffusion. Within the transport code the molecular diffusion coefficients are calculated according to Banks and Kockarts [1973]. We use a fixed eddy diffusion coefficient profile, which has a maximum of $1.3 \times 10^6\ cm^2\ s^{-1}$ at 102 km.

[15] The SIC model can be run either in a steady-state or a time-dependent mode. For this study we used the time-dependent mode which exploits the semi-implicit Euler method for stiff sets of equations [Press et al., 1992] to advance the concentrations of the chemical species in time. Vertical transport and chemistry are advanced in 15-min intervals during which background atmosphere and external forcing are kept constant. In the beginning of every interval all modeled neutrals, except the short-lived constituents $O(^1D)$ and $N(^2D)$, are transported. Next, new values for solar zenith angle, background atmosphere, and ionization/dissociation rates due to solar radiation and particle precipitation are calculated. Finally, the chemistry is advanced.

3.1. Proton Forcing

[16] We have undertaken ionization rate calculations using GOES-11 satellite proton flux data, available from the NOAA National Geophysical Data Center World Wide Web server at www.ndgc.noaa.gov/stp/stp.html. GOES satellites measure integrated proton fluxes above seven threshold values: 1, 5, 10, 30, 50, 60, and 100 MeV. An integrated proton flux can be described by an exponential rigidity relation [Freier and Webber, 1963], which we used to convert the GOES measurements to differential proton fluxes over the range 600 keV to 2000 MeV. The ionization rate calculation is based on proton energy-range measurements in standard air [Bethe and Ashkin, 1953]. The energy-range relation for protons can be written

$$R(E) = aE^b, \tag{1}$$

where R is the range, E is the proton energy, and a and b are parameters set by measurements. Using the following algorithm, originally presented by Reid [1961], we calculate energy deposition rates on each altitude: The stopping power of a proton with initial energy E and pitch angle θ at altitude h is

$$\frac{dE}{dx} = \left(\frac{dR(E,h,\theta)}{dE}\right)^{-1}, \tag{2}$$

where

$$R(E,h,\theta) = R(E) - \frac{1}{n_0}\int_h^\infty \frac{n(h)}{\cos\theta}dh \tag{3}$$

is the remaining range at altitude h. The total concentrations n_0 and n(h) are taken at ground level and at altitude h, respectively. The last term in equation (3) is the standard air range, i.e., energy, lost by a proton in penetrating the atmosphere down to altitude h. By dividing equation (2) by mean ionization energy $\Delta\epsilon$, taken to be 36 eV [see, e.g., Rees, 1989, p. 40], and multiplying by the proton flux F(E) and then integrating over energies and angles, we get the total ionization rate for each altitude from

$$Q = \frac{1}{\Delta\epsilon}\int\int\int\left(\frac{dE}{dx}\right)F(E)\sin\theta\ d\theta d\phi dE. \tag{4}$$

The total ionization rate is divided between N_2, O_2, and O, according to their relative concentrations and cross sections [Rees, 1982]. Then these three ionization rates are divided between the ionization and dissociative ionization processes using the branching ratios given by Jones [1974] to obtain the production/loss rates for the individual species.

Table 2. $N(^2D)$-Producing Reactions, Rates/Rate Coefficients, and Branching Ratios Used in the SIC Model[a]

Reaction	Rate/Rate Coefficient, $cm^{-3}\ s^{-1}$	$N(^2D)$: $N(^4S)$	Sources
$e_s^* + N_2 \rightarrow N + N + e_s^*$	$0.80 \times Q$	0.60: 0.40	Zipf et al. [1980]; Rusch et al. [1981]
$p_p^* + N_2 \rightarrow N + N^+ + p_p^* + e_s^*$	$0.19 \times Q$	0.50: 0.50	Jones [1974]; Porter et al. [1976]; Rees [1982]
$NO^+ + e \rightarrow N + O$	$4.2 \times 10^{-7} \times (300/T)^{0.85}$	0.85: 0.15	Bates [1988]; Vejby-Christensen et al. [1998]
$N^+ + O_2 \rightarrow N + O_2^+$	2.0×10^{-10}	0.65: 0.35	Rees [1989]
$N_2^+ + O \rightarrow N + NO^+$	$1.4 \times 10^{-10} \times (300/T)^{0.44}$	1.00: 0.00	McFarland et al. [1974]
$N_2^+ + e \rightarrow N + N$	$1.8 \times 10^{-7} \times (300/T)^{0.39}$	0.50: 0.50	Mul and McGowan [1979]

[a]Notation: p_p^* = primary proton, e_s^* = secondary electron, e = thermal electron, and Q = total ionization rate due to proton precipitation.

[17] As a results of proton precipitation, atomic nitrogen is produced from N_2 in dissociative ionization by primary protons and in dissociation by secondary electrons. In addition, ion chemistry produces both atomic nitrogen and nitric oxide. For the production of atomic nitrogen it is important to consider the branching between the ground state $N(^4S)$ and the excited state $N(^2D)$ because the former destroys while the latter produces NO. Table 2 lists the reactions producing $N(^2D)$ in the SIC model. HO_x production is a result of ionization, water cluster ion formation, and subsequent neutralization. The SIC model considers also an additional route to HO_x production via HNO_3 formation due to ion-ion recombination and subsequent photodissociation of HNO_3 [Solomon et al., 1981; Aikin, 1997].

3.2. Modeling of the October–November 2003 SPEs

[18] For this study, we selected the location 70°N/0°E and an altitude range of 20–120 km. Before modeling the October–November 2003 solar proton events, we set up the SIC model for quiet time conditions equivalent to late October by repeating a diurnal cycle until convergence, i.e., no significant change between the last and previous cycle. This initialization of the model typically requires 8–12 cycles.

[19] The level of solar illumination is relatively low during the modeled period. The solar zenith angle at noon is about 84° so that the photodissociation processes are diminished particularly in the stratosphere. This results in a relatively low production of photolysis products, such as $O(^1D)$. At the stratopause, the sunrise and sunset occur at approximatively 0700 LT and 1700 LT. The zenith angle is 90° at about 0845 LT and 1515 LT.

[20] The minor gases of the background atmosphere are an important part of the modeling because they can be used to control the initial level of the modeled constituents. For example, changes in amounts of H_2O (source of HO_x), N_2O (source of NO_x), or ClO_x could affect the amount of ozone. Test runs for this particular modeling case indicate that the amount of ozone is quite insensitive to changes in N_2O because the reaction with $O(^1D)$, producing NO, is diminished due to relatively low level of solar radiation. On the other hand, changes in H_2O and ClO_x have a clear effect on ozone at certain altitudes.

[21] During the initialization, to improve comparison with GOMOS ozone measurements, we made adjustments to the model background atmosphere and diffusion boundary conditions: (1) Daytime Cl and ClO values given by Shimazaki [1984] were doubled around 30 km where the sensitivity of ozone to changes in ClO_x is largest, new values being 6.1×10^4 and 1.0×10^8 cm^{-3}, respectively. (2) Below 83 km the water vapor amount was increased from the default 5 ppmv to 7.5 ppmv between 20 and 70 km. At 71 and 83 km values 7.5 and 3 ppmv were used, respectively, and a linear interpolation in between. (3) At 120 km the atomic oxygen downward flux was set to 10^{11} $cm^{-2}s^{-1}$. (4) Two reaction rate coefficients were adjusted; see Table 1. The comparison with GOMOS is presented in section 5.2.

[22] After initialization, we introduced the proton forcing, i.e., included ionization rates calculated from GOES proton flux data. The fluxes were taken to be isotropic. The location of our modeling (70°N/0°E) corresponds to a high magnetic latitude of 68°N. Therefore as a first approximation, we can neglect the magnetic cutoff effects [see, e.g., Hargreaves, 1992, pp. 351–361]. Figure 1 shows the calculated ionization rates for 26 October to 7 November.

[23] We started the modeling at 0000 UT on 26 October and modeled the event until 7 November, 0000 UT. We call this the proton run. We also repeated the same modeling run without proton forcing. This we call the control run.

4. Measurements

4.1. Subionospheric VLF Propagation

[24] Very low frequency (VLF) (3–30 kHz), long-wave radio signals are used in communication systems, for example, between ground stations and submarines. The signals used in communication systems are generated by high power transmitters but VLF signals can also be generated by natural processes such as lightning. The VLF signals propagate in the waveguide formed by the

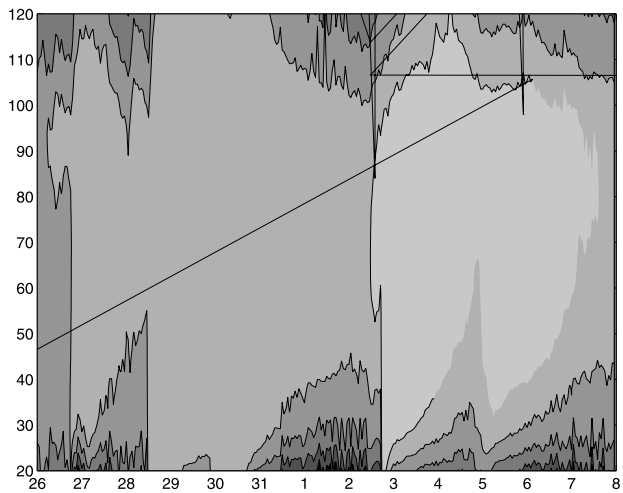

Earth's surface and the bottom of the Earth's ionosphere located between 50 and 100 km [Barr et al., 2000], that is, subionospherically. Therefore changes in the ionosphere produce changes in the received amplitude and phase of the VLF signals.

[25] The signals coming from distant locations can be monitored by VLF receivers set up in different locations around the Earth. In this study, we have used the VLF receiver at Ny Ålesund, Svalbard, Norway (78°54′N, 11°53′E, L = ∼18), to monitor the VLF signal coming from Reykjavik, Iceland (NRK, 37.5 kHz). The great circle path from NRK to Ny Ålesund (see Figure 2) crosses through the magnetic polar cap area, close to the SIC modeling location, allowing the signal to be influenced by ionospheric changes caused by the proton precipitation.

[26] To study the signal propagation conditions, we have used the Long Wave Propagation Code (LWPC) [Ferguson and Snyder, 1990] provided by the Naval Ocean Systems Center (NOSC) to model the NRK VLF signal. To calculate the signal amplitude and phase at the reception point, LWPC needs electron density profile parameters that define the ionospheric conditions. These parameters are calculated from electron density profiles provided by the SIC model results [Clilverd et al., 2005] made during the proton run. Thus we are able to compare the observed NRK to Ny Ålesund amplitude variations during SPE conditions with the output of the LWPC propagation model. The LWPC calculations are done for the same NRK to Ny Ålesund propagation path and the same transmitter frequency, using the SIC electron density profiles to define the changing ionospheric conditions during the SPE.

4.2. NO_2 and O_3 Measurements by GOMOS

[27] GOMOS is a stellar occultation instrument on board the European Space Agency's Envisat satellite [Bertaux et al., 1991, 2004; Kyrölä et al., 2004]. Launched from French Guiana on 1 March 2002, Envisat carries a total of 10 instruments. These include three atmospheric chemistry instruments: GOMOS, MIPAS (Michelson Interferometer for Passive Atmospheric Sounding), and SCIAMACHY (SCanning Imaging Absorption SpectroMeter for Atmospheric CHartographY).

[28] GOMOS consists of a star tracker, used to guide the pointing system, two spectrometers working in the ultraviolet-visible-near-infrared (UV-vis: 248–690 nm and IR: 750–776 nm, 916–956 nm), and two photometers (blue: 470–520 nm and red: 650–700 nm). GOMOS measures the light of a star as the star descends through the Earth's atmosphere. The incoming light travels through the atmosphere and is absorbed and scattered by various molecules along its path. Knowing the absorption features of the different atmospheric gases their altitude profiles can be calculated using advanced inversion methods [Kyrölä et al., 1993]. The wide spectral range of GOMOS enables inversion for vertical profiles of O_3, NO_2, NO_3, H_2O, O_2, neutral density, and aerosols. The two photometers allow measurement of temperature profiles with high vertical resolution and can also be used to study turbulence in the atmosphere. The altitude range of the measurements is between 10 and 100 km for ozone and, because of their low abundance in the mesosphere and above, 10–50 km for the other gases. The measurement vertical resolution is better than 1.7 km.

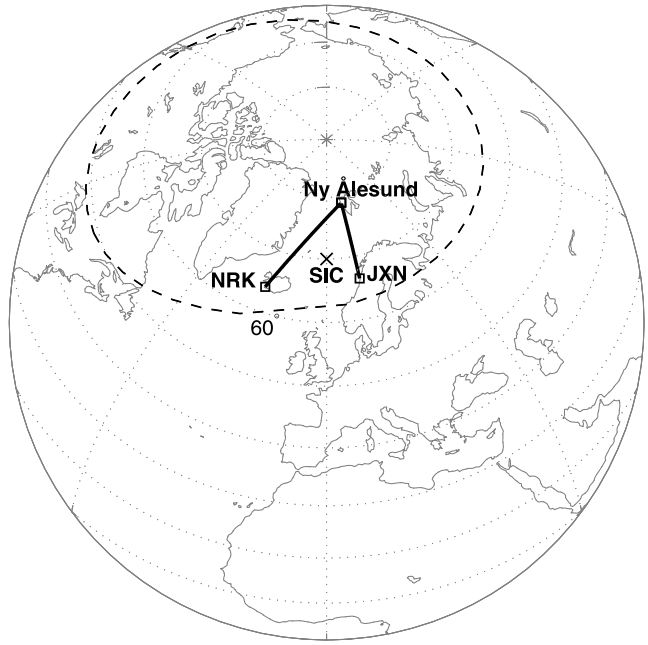

Figure 2. Great circle paths of the VLF signals from NRK (Iceland) and JXN (Norway) to Ny Ålesund. The dashed line is the geomagnetic latitude 60°. SIC model point is marked with an X. The dotted lines are latitude and longitude isolines with 10° and 45° spacing, respectively.

Using stars as a light source instead of sunlight, measurements from both dayside and nightside of the Earth can be attained (henceforth referred as bright limb and dark limb measurements, respectively). In addition to stellar occultation, the main measurement technique, GOMOS is also able to measure scattered solar light in the Earth limb.

[29] The altitude range and error of GOMOS measurements are dependent on the star temperature and magnitude. For example, in the case of ozone the bright and hot stars give best accuracy with typical uncertainties of the order of 5% around both the primary and secondary maximum of ozone. The stratospheric ozone product of GOMOS has been extensively validated by Meijer et al. [2004], who concluded that GOMOS nighttime measurements between 19 and 64 km agree very well with ground-based and balloon-sonde measurements, showing a small negative bias of 2.5–7.5%. On the other hand, GOMOS data quality was found to be strongly dependent on the illumination of the limb through which the star is observed, the bright limb measurements showing a strong negative bias of 18–33% and a limited altitude range.

[30] In this study we have used GOMOS measurements from the Northern Hemisphere polar area from geographic latitudes 65° to 75° before and during the great storm period of October–November 2003. All NO_2 and ozone profiles were produced using GOMOS processing prototype version 6.0a. We selected stars with magnitude better than 2.834 and required the star temperature to be higher than 7000 K and 10,000 K for the dark and bright limb, respectively. We are aware of the negative bias in the daytime ozone measurements. However, we assume that by selecting the measurements in such a way that the difference in solar zenith angle is small during the period of the study, the

daytime measurements should have equal relative bias allowing the change of ozone during the proton event to be monitored correctly.

5. Results and Comparison

[31] The modeled response of the middle atmosphere to the solar proton event is presented in Figure 3. Negative ion concentrations are enhanced by several orders of magnitude during the periods of extreme forcing. This is directly dependent on the ionization rate and thus can be used for monitoring of the magnitude of the forcing below 80 km. The events on 26–27 October, 28–31 October, 2–4 November, and 5–6 November are easily identified.

[32] HO_x ($H + OH + HO_2$) displays a strong diurnal cycle below 80 km. The HO_x response to proton forcing is clear at night, with order-of-magnitude changes on 29–31 October and 3 November. During daytime the natural production from water vapor is high and thus SPE effects can only be identified during the most intense ionization periods [see also Solomon et al., 1981]. HO_x recovers relatively fast (in a day), which is demonstrated after the end of the largest events, on 1 November as well as on 5 November. Above 80 km the impact of protons is small on HO_x levels. It should be noted that around 70 km the background altitude profiles of H_2O_2 used in the model could result in an overestimation of the HO_x concentration and ozone depletion by a few percent.

[33] NO_x ($N + NO + NO_2$) displays a quite different response from that of HO_x. Once affected by proton forcing, NO_x stays at an elevated level. The recovery is slow because of the long chemical lifetime of NO_x especially at high solar zenith angles [see, e.g., Brasseur and Solomon, 1986, pp. 256]. On 26–27 October, NO_x is enhanced at 60–80 km, while the largest event on 28–31 October leads to enhancements of several hundred per cent at altitudes above 40 km. In contrast, the effect of the 2–4 November and 5–6 November events is small on the already elevated NO_x levels.

[34] The bottom of Figure 3 shows the relative difference in O_x ($O + O_3$) between the proton and control runs, i.e., $100 \times (\text{proton/control} - 1)$. O_x is depleted between 40 and 85 km, with clear differences in the magnitude of depletion with respect to the diurnal cycle and altitude. Substantial O_x loss occurs at sunset of 28 October. During night the O_x depletion is moderate because most of the O_x loss cycles depend on the amount of atomic oxygen. O_x does not recover, however, because it is not significantly produced at night. Even greater loss is seen at sunrise of 29 October, which is followed by a recovery at 55–75 km during the noon and afternoon hours. The maximum depletion is reached just after sunset, with a 95% reduction in the O_x values at 78 km. During daytime on 30 October, O_x partly recovers but is again depleted during sunset. The next day, 31 October, a recovery again occurs after which the O_x values stay on 0–30% lower level until the next event on 2–4 November.

[35] O_x depletion is driven by the proton forcing. The amount and altitude distribution of the depletion is dependent on the flux and energy of the protons. It is also dependent on the diurnal variation of HO_x. The HO_x reaction cycles have the greatest impact on O_x during sunrise and sunset when (1) there is significant enhancement of HO_x due to proton forcing and (2) atomic oxygen is available. O_x recovery occurs during noon hours, when the photodissociation processes are most effective, because of the high background production of HO_x and the production of O_x at that time. The recovery is relatively slow and displays an altitude dependence, i.e., the recovery is generally faster at higher altitudes, because the solar zenith angle is high throughout the day. NO_x does not show significant diurnal variation but the reaction cycles destroying O_x require atomic oxygen. Therefore the NO_x cycles are most effective during daytime. The nearly constant 20% O_x depletion at 50 km, beginning on 29 October at noon and lasting beyond 6 November, is for the most part due to the increase and persistence of NO_x.

5.1. VLF Signal Modeling and Comparison

[36] The average quiet-day behavior (Quiet Day Curve, QDC) of the NRK signal received at Ny Ålesund was determined from the average of 4 days before and after the period of high magnetic activity. This is shown in Figure 4a as the solid line. The QDC shows an essentially "v"-shaped variation with a minimum amplitude at 1100 UT and a maximum at 1900 UT. The total amplitude change is about 8 dB throughout the day. The equivalent QDC determined from calculating the NRK propagation conditions with the LWPC VLF propagation code (diamonds), using the quiet-time SIC electron density profiles to define the ionospheric profile [e.g., Clilverd et al., 2005], shows low amplitudes during the daytime (0700–1600 UT), and high amplitudes during the night (1700–0600 UT). The SIC based amplitude range is about 7 dB. Clearly, the quiet-time SIC model is providing electron density profiles that can well represent the radio propagation conditions inferred from observing the behavior of the NRK signal. Although not shown here, we also studied the Norway (JXN, 16.4 kHz) signal to Ny Ålesund in a similar way (see Figure 2 for path information). Very good agreement was found between the observations and the modeling in this case.

[37] The SPE studied here starts at 1215 UT, on 28 October. Figure 4b shows that the NRK signal from the first half of the day (solid line) initially follows closely the QDC determined previously (dashed line). However, just prior to the SPE start the signal is elevated in amplitude relative to the QDC as a result of the precipitation caused by the previous small SPE that occurred on 26 October.

[38] The SPE proton fluxes peak on 29 October (see Figure 1), before gradually returning to low levels by the end of 31 October. During this period the effect of the SPE on the observed NRK amplitude can be seen as varying signal absorption, with values exceeding QDC levels at times, and returning to close to QDC levels on 31 October. This is shown in detail in Figure 4c by the solid line. The calculated SPE effect on VLF propagation conditions driven by the changing SIC model electron density profiles is also shown in this figure (diamonds). These have been calculated using the LWPC VLF propagation code. The calculations show good agreement with the observations, in that there is initially absorption of the signal to about −4 dB, followed by varying levels of absorption as the signals recover to QDC levels during 31 October. Such good agreement suggests that the SIC model is capturing

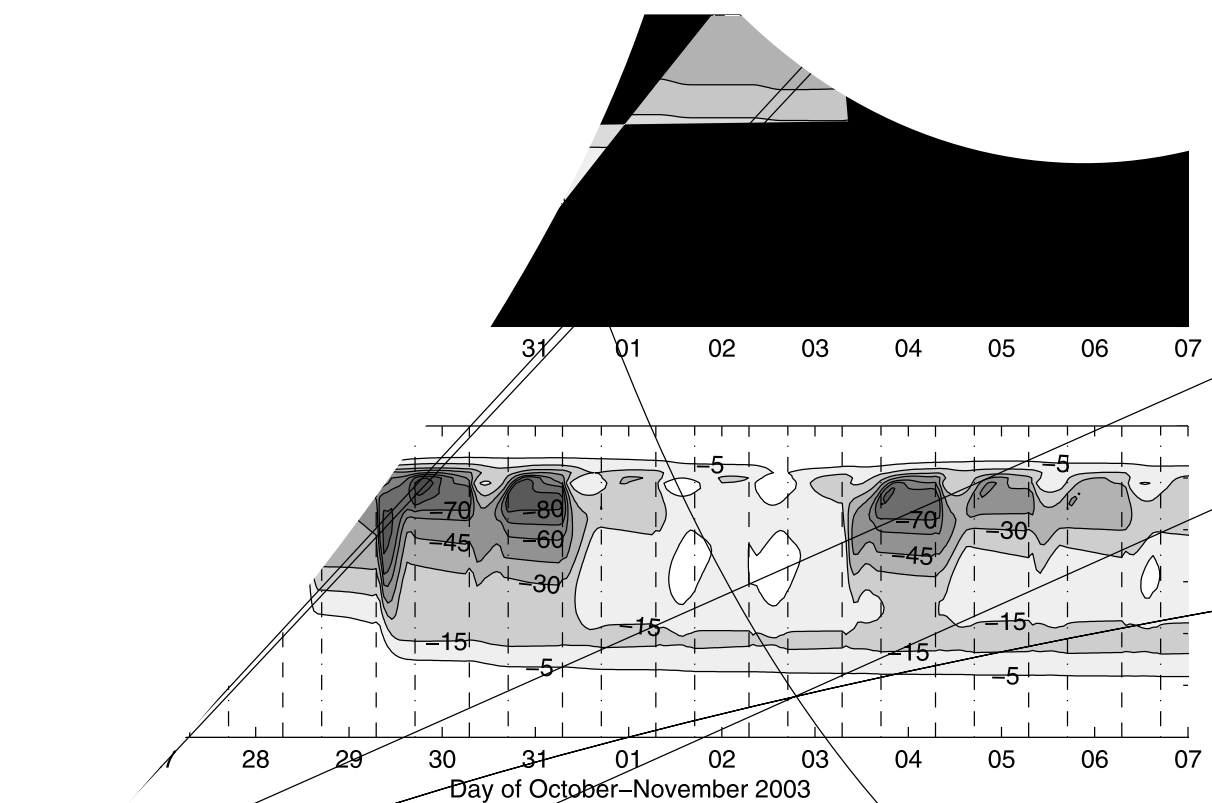

Figure 3. Middle atmospheric response to the proton event (modeling results). From top down: (a) Negative ion concentration [$\log_{10}(\mathrm{cm}^{-3})$], (b) HO_x concentration [$\log_{10}(\mathrm{cm}^{-3}$ $_x$ concentration [$\log_{10}(\mathrm{cm}^{-3})$], (d) relative change of O_x [%], i.e., 100 × (proton/control − 1). The tick marks on the horizontal axis indicate the beginning, i.e., 0000 LT, of each day. The approximative times of sunrise (dash) and sunset (dash-dot) are marked with vertical lines.

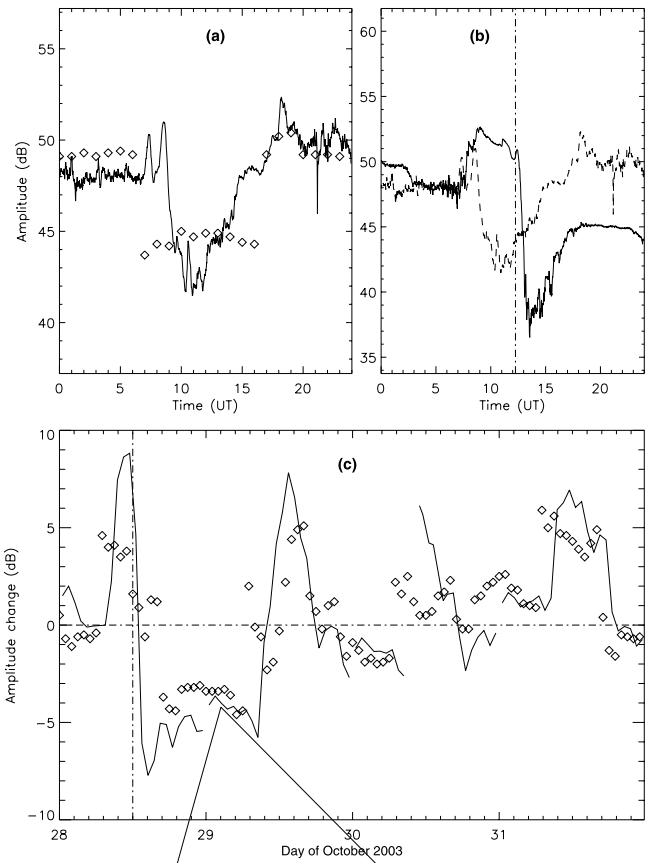

Figure 4. (a) The average nondisturbed diurnal variation (QDC) of NRK received at Ny Ålesund (solid line) and the ...ivalent values calculated using the electron density ... from the SIC quiet-time runs (diamonds). (b) The ...he SPE on the NRK signal during 28 October ...e). The QDC is shown as a dashed line, and ...me of the SPE is indicated by the vertical ...e effect of the SPE on NRK signals ...uring the 4 days of high prot... ...ivalent values calculate... ...lectron densit... ...tracted...

...magnitude ...ic accuracy of the ...ecomes worse with increas-

ing altitude due to decreasing abundance of NO_2, such that the upper limit of NO_2 measurements is usually considered to be at 45–50 km. The scatter of the measurements above 40 km indicates that the uppermost GOMOS NO_2 measurements may be at this noise floor. Differences in the diurnal phase of NO_2 cannot explain the scatter because the measurements were obtained at a virtually constant solar zenith angle. On 3 November the agreement between the NO_2 profiles is better. The profiles are very similar in shape and differ in magnitude by less than 50% between 35 and 60 km. The proton forcing brings the model and measurements into a better agreement. This indicates to us that the modeling of SPE effects, at least the production of NO_x, is generally correct. Also, the larger amount of NO_2 at the higher altitudes seems to give more accurate measurements by GOMOS so that for special cases of enhanced production it is possible to extend the altitude range of NO_2 measurements above 50 km.

[41] Nighttime ozone profiles (Figure 6, left) show generally a good agreement below 40 km. On the other hand, SIC seems to overestimate the amount of ozone between 40 and 80 km by up to 100% and underestimate it around the secondary maximum. The situation is not changed by the solar proton events, as the comparison of 3 November profiles shows. However, the comparison of

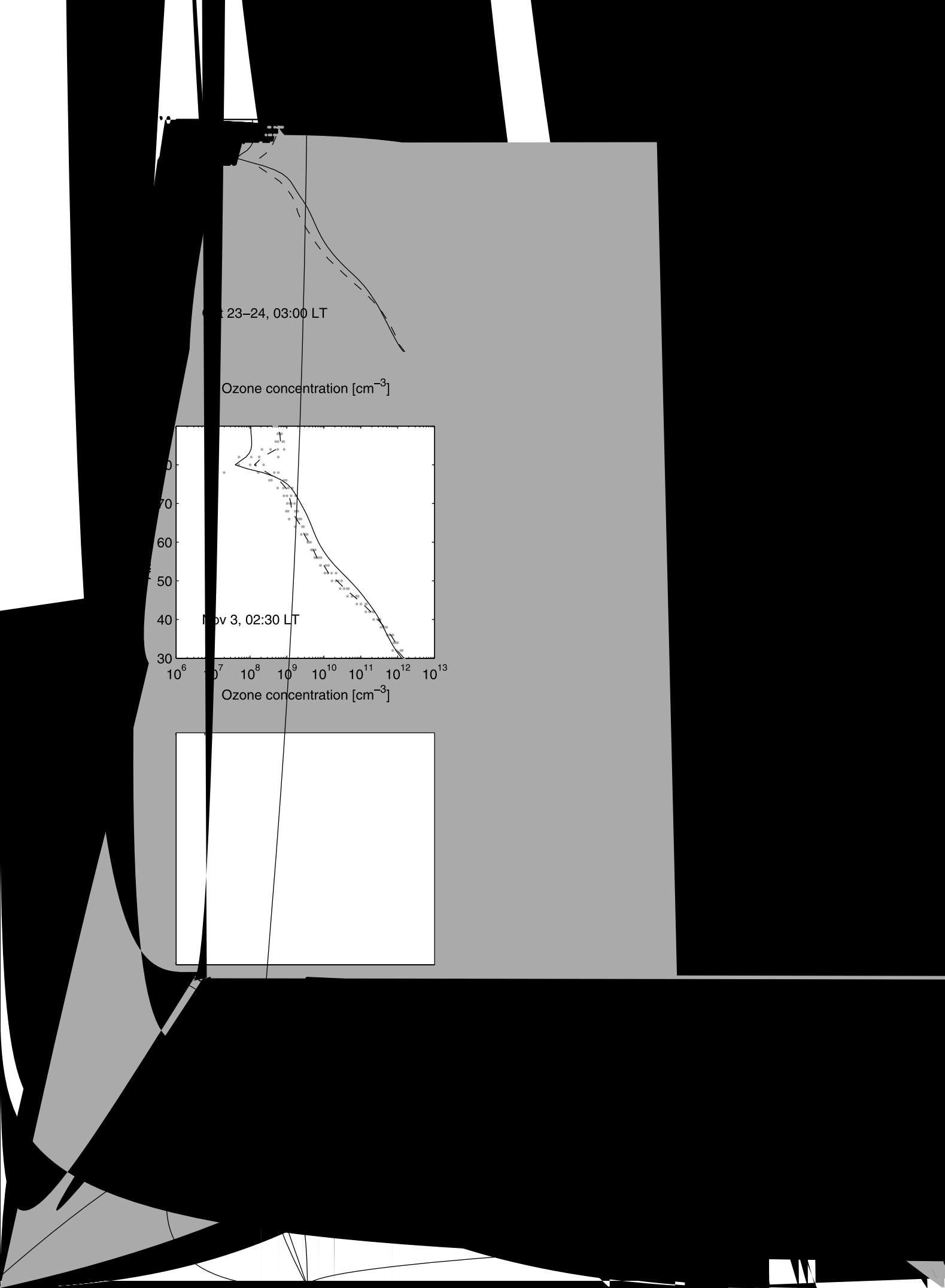
t 23–24, 03:00 LT
Ozone concentration [cm^{-3}]
70
60
50
40
30
ov 3, 02:30 LT
10^{6}
10^{7}
10^{8}
10^{9}
10^{10}
10^{11}
10^{12}
10^{13}
Ozone concentration [cm^{-3}]

Figure 7. Relative change of ozone between 23 October and 5 November for altitudes 50, 60, and 70 km. The GOMOS values are weighted zonal averages for latitudes 65–75°N. The reference values, separate for daytime and nighttime, are averages of the 23–25 October measurements. The SIC model values present a comparison between the control and proton runs, i.e., 100 × (proton/control – 1). Solid curve represents SIC model results, open circle represents GOMOS daytime measurements, asterisk represents GOMOS nighttime measurements. The vertical solid lines show statistical error estimates for the GOMOS values. The tick marks on the horizontal axis indicate the beginning, i.e., 0000 LT, of each day and the approximative times between sunset and sunrise have a gray shading. The three dotted horizontal lines at the bottom of each panel indicate the magnitude of ionization due to proton precipitation: One line $>10^2$, two lines $>10^3$, and three lines $>10^4$ $cm^{-3}s^{-1}$.

[42] Daytime ozone profiles (Figure 6) show change agree nitude agreement between 60 and 70 km. Below the m es overestimates the amount of ozone predicting 100% h km values between 35 and 50 km. A part of this differen probably due to the negative bias in GOMOS day measurements (see section 4.2). The model shows a of ozone significantly lower values around the secondary maxi el is pres ed in of ozone. On 3 November the situation is similar, alth s, 50, 60, and 70 n. The the comparison between 40 and 50 km is slightly w between GOMOS measureme and SIC the model showing about 120% higher values. The profiles mod is generally good, althoug n the initial

effect of the 29 November event seems to be underestimated by the model. It is obvious that the SIC model is able to represent reasonably well the day-to-day changes in ozone due to the proton forcing. The diurnal variation of ozone depletion increases with increasing altitude because of increasing dependency on the HO_x reactions and faster daytime production of O_x. At 50 km the variation is not significant while at 70 km the magnitude of the depletion can differ within a day by several tens percent, depending on the local time considered. The largest depletions occur during sunrise hours. Therefore an instrument measuring solely at that time would generally overestimate the magnitude of ozone depletion in the middle mesosphere [see also Aikin and Smith, 1999].

6. Conclusions

[44] We have studied the short-term effects of the October–November 2003 solar proton events on the middle atmosphere. Model results as well as VLF and GOMOS measurements indicate significant changes in the D-region ionosphere, enhancement in concentrations of odd hydrogen and odd nitrogen, and depletion of ozone in the middle atmosphere. The ozone depletion displays a clear diurnal cycle in the middle mesosphere as a result of being modulated by the HO_x cycle but also due to faster ozone production, i.e., recovery, at higher altitudes.

[45] We have used the Sodankylä Ion Chemistry Model electron densities as an input to the LWPC model to model the behavior of the VLF signal from the NRK transmitter to Ny Ålesund and compared them with the equivalent observations. The results show a good agreement between the modeled and the measured VLF signal, thus indicating that SIC is correctly calculating the ionization and the electron densities. This suggests that taking into account ionization from only proton precipitation and secondary electrons but not from additional electron precipitation is a good assumption for the model SPE study.

[46] During the events, modeled HO_x and NO_x values are both enhanced drastically but display a quite different recovery. HO_x show a rapid response to proton forcing below 80 km, which is most visible at night with order-of-magnitude enhancements, and a quick recovery after one quiet day. NO_x is affected above 40 km sustaining its level after proton forcing and continuing to affect ozone beyond our model calculation [Seppälä et al., 2004]. The comparison of NO_2 profiles shows agreement between the SIC calculation and GOMOS measurements, especially after the onset of the event, indicating a generally correct modeling of NO_x production.

[47] Model results show that ozone is depleted between 40 and 85 km during the solar proton events. The largest relative changes, due to HO_x increase, occur just after sunset on 29 October between 75 and 80 km, with a maximum depletion by 95%. The magnitude of the ozone depletion is dependent not only on the flux and energy of the protons but also on the diurnal cycle of HO_x constituents. A relatively fast partial recovery of ozone occurs at 60–85 km after a reduction in the proton forcing. Around the stratopause a persistent 20% decrease due to NO_x increase/persistence is seen after the largest event on 28–31 November, lasting until the end of our modeling calculation (6 November). These model results are in good agreement with ozone measurements of the GOMOS instrument.

[48] **Acknowledgments.** The work of PTV was partly supported by the Academy of Finland through the ANTARES space research programme. The work of AS was supported by the Academy of Finland (MAIST: Middle Atmosphere Interactions with Sun and Troposphere). CFE acknowledges financial support through the European Community's Human Potential Programme under contract HPRN-CT-2002-00216, CAL. PTV thanks Simon Chabrillat for providing the vertical diffusion code and Donal Murtagh for providing the transmission and O_2 cross-section code for the Schumann-Runge bands.

[49] Arthur Richmond thanks Arthur C. Aikin and Miriam Sinnhuber for their assistance in evaluating this paper.

References

Aikin, A. C. (1997), Production of stratospheric HNO_3 by different ion-molecule reaction mechanisms, J. Geophys. Res., 102, 12,921–12,926.

Aikin, A. C., and H. J. P. Smith (1999), Mesospheric constituent variations during electron precipitation events, J. Geophys. Res., 104, 26,457–26,472.

Banks, P. M., and G. Kockarts (1973), Aeronomy, vol. B, chap. 15, Elsevier, New York.

Barr, R., D. L. Jones, and C. J. Rodger (2000), ELF and VLF radio waves, J. Atmos. Terr. Phys., 62, 1689–1718.

Bates, D. R. (1988), Recombination in the normal E and F layers of the ionosphere, Planet. Space Sci., 36, 55–63.

Bertaux, J. L., G. Megie, T. Widemann, E. Chassefiere, R. Pellinen, E. Kyrölä, S. Korpela, and P. Simon (1991), Monitoring of ozone trend by stellar occultations: The GOMOS instrument, Adv. Space Res., 11(3), 237–242.

Bertaux, J. L., et al. (2004), First results on GOMOS/Envisat, Adv. Space Res., 33, 1029–1035.

Bethe, A. H., and J. Ashkin (1953), Passage of radiations through matter, in Experimetal Nuclear Physics, vol. 1, edited by E. Segre, pp. 166–251, John Wiley, Hoboken, N. J.

Brasseur, G., and S. Solomon (1986), Aeronomy of the Middle Atmosphere, 2nd ed., Springer, New York.

Burns, C. J., E. Turunen, H. Matveinen, H. Ranta, and J. K. Hargreaves (1991), Chemical modeling of the quiet summer D- and E-regions using EISCAT electron density profiles, J. Atmos. Terr. Phys., 53, 115–134.

Chabrillat, S., G. Kockarts, D. Fonteyn, and G. Brasseur (2002), Impact of molecular diffusion on the CO_2 distribution and the temperature in the mesosphere, Geophys. Res. Lett., 29(15), 1729, doi:10.1029/2002GL015309.

Clilverd, M. A., C. Rodger, T. Ulich, A. Seppälä, E. Turunen, A. Botman, and N. Thomson (2005), Modelling a large solar proton event in the southern polar cap, J. Geophys. Res., doi:10.1029/2004JA010922, in press.

Crutzen, P. J., I. S. A. Isaksen, and G. C. Reid (1975), Solar proton events: Stratospheric sources of nitric oxide, Science, 189, 457–458.

Cummer, S. A., T. F. Bell, U. S. Inan, and D. L. Chenette (1997), VLF remote sensing of high energy auroral particle precipitation, J. Geophys. Res., 102(11), 7477–7484.

Fell, C., J. I. Steinfeld, and S. Miller (1990), Quenching of N(2D) by O(3P), J. Chem. Phys., 92, 4768–4777.

Ferguson, J. A., and F. P. Snyder (1990), Computer programs for assessment of long wavelength radio communications, Tech. Doc. 1773, Natl. Ocean Syst. Cent., Alexandria, Va.

Freier, P. S., and W. R. Webber (1963), Exponential rigidity spectrums for solar-flare cosmic rays, J. Geophys. Res., 68, 1605–1629.

Fuller-Rowell, T. J. (1993), Modeling the solar cycle change in nitric oxide in the thermosphere and upper mesosphere, J. Geophys. Res., 98, 1559–1570.

Hargreaves, J. K. (1992), The Solar-Terrestrial Environment, Cambridge Atmos. and Space Sci. Ser., Cambridge Univ. Press, New York.

Hedin, A. E. (1991), Extension of the MSIS thermospheric model into the middle and lower atmosphere, J. Geophys. Res., 96, 1159–1172.

Jackman, C. H., and R. D. McPeters (1985), The responce of ozone to solar proton events during -277.2(ambrii0.63I-279d[(J.)-3TDity)-579.9(t)-0.ore(paa)n,

due to the July 2000 solar proton events, Geophys. Res. Lett., 28, 2883–2886.
Jones, A. V. (1974), Aurora, Springer, New York.
Kazil, J., E. Kopp, S. Chabrillat, and J. Bishop (2003), The University of Bern Atmospheric Ion Model: Time-dependent modeling of the ions in the mesosphere and lower thermosphere, J. Geophys. Res., 108(D14), 4432, doi:10.1029/2002JD003024.
Koppers, G. A. A., and D. P. Murtagh (1996), Model studies of the influence of O2 photodissociation parameterizations in the Schumann-Runge bands on ozone related photolysis in the upper atmosphere, Ann. Geophys., 14, 68–79.
Kyrölä, E., E. Sihvola, Y. Kotivuori, M. Tikka, T. Tuomi, and H. Haario (1993), Inverse theory for occultation measurements: 1. Spectral inversion, J. Geophys. Res., 98, 7367–7381.
Kyrölä, E., et al. (2004), GOMOS on Envisat: An overview, Adv. Space Res., 33, 1020–1028.
McEwan, M. J., and L. F. Phillips (1975), Chemistry of the Atmosphere, 309 pp., Halsted Press, New York.
McFarland, M., D. L. Albritton, F. C. Fehsenfeld, E. E. Ferguson, and A. L. Schmeltekopf (1974), Energy depencence and branching ratio of the N_2^+ + O reaction, J. Geophys. Res., 79, 2925.
McPeters, R. D., and C. H. Jackman (1985), The response of ozone to solar proton events during solar cycle 21: The observations, J. Geophys. Res., 90, 7945–7954.
Meijer, Y. J., et al. (2004), Pole-to-pole validation of ENVISAT/GOMOS ozone profiles using data from ground-based and balloon-sonde measurements, J. Geophys. Res., 109, D23305, doi:10.1029/2004JD004834.
Minschwaner, K., and D. E. Siskind (1993), A new calculation of nitric oxide photolysis in the stratosphere, mesosphere, and lower thermosphere, J. Geophys. Res., 98, 20,401–20,412.
Mul, P. M., and J. W. McGowan (1979), Merged electron-ion beam experiments. III - Temperature dependence of dissociative recombination for atmospheric ions NO/+/, O2/+/, and N2/+/, J. Phys. B, 12, 1591–1601.
Ohshio, M., R. Maeda, and H. Sakagami (1966), Height distribution of local photoionization efficiency, J. Radio Res. Lab., 13, 245.
Patterson, J. D., T. P. Armstrong, C. M. Laird, D. L. Detrick, and A. T. Weatherwax (2001), Correlation of solar energetic protons and polar cap absorption, J. Geophys. Res., 106, 149–163.
Porter, H. S., C. H. Jackman, and A. E. S. Green (1976), Efficiencies for production of atomic nitrogen and oxygen by relativistic proton impact in air, J. Chem. Phys., 65, 154–167.
Press, W. H., S. A. Teukolsky, W. T. Vetterling, and B. P. Flannery (1992), Numerical Recipes in FORTRAN, The Art of Scientific Computing, Clarendon, Oxford, U.K.
Randall, C. E., D. E. Siskind, and R. M. Bevilacqua (2001), Stratospheric NO_x enhancements in the southern hemisphere vortex in winter/spring of 2000, Geophys. Res. Lett., 28, 2385–2388.
Reames, D. V. (1999), Particle acceleration at the Sun and in the heliosphere, Space Sci. Rev., 90, 413–491.
Rees, M. H. (1982), On the interaction of auroral protons with the Earth's atmosphere, Planet. Space Sci., 30, 463–472.
Rees, M. H. (1989), Physics and Chemistry of the Upper Atmosphere, Cambridge Atmos. and Space Sci. Ser., Cambridge Univ. Press, New York.
Reid, G. C. (1961), A study of the enhanced ionization produced by solar protons during a polar cap absorbtion event, J. Geophys. Res., 66, 4071–4085.
Reid, G. C., S. Solomon, and R. R. Garcia (1991), Response of the middle atmosphere to the solar proton events of August–December, 1989, Geophys. Res. Lett., 18, 1019–1022.
Rietveld, M. T., E. Turunen, H. Matveinen, N. P. Goncharov, and P. Pollari (1996), Artificial periodic irregularities in the auroral ionosphere, Ann. Geophys., 14, 1437–1453.
Rusch, D. W., J.-C. Gérard, S. Solomon, P. J. Crutzen, and G. C. Reid (1981), The effect of particle precipitation events on the neutral and ion chemistry of the middle atmosphere – I. Odd nitrogen, Planet. Space Sci., 29, 767–774.
Sander, S. P., et al. (2003), Chemical kinetics and photochemical data for use in stratospheric modeling: Evaluation 14, JPL Publ. 02-25, Jet Propul. Lab., Calif. Inst. of Technol., Pasadena, Calif.
Seppälä, A., P. T. Verronen, E. Kyrölä, S. Hassinen, L. Backman, A. Hauchecorne, J. L. Bertaux, and D. Fussen (2004), Solar proton events of October–November 2003: Ozone depletion in the northern hemisphere polar winter as seen by GOMOS/Envisat, Geophys. Res. Lett., 31, L19107, doi:10.1029/2004GL021042.
Shimazaki, T. (1984), Minor Constituents in the Middle Atmosphere, Dev. in Earth and Planet. Phys., vol. 6, Springer, New York.
Siskind, D. E., D. J. Strickland, R. R. Meier, T. Majeed, and F. G. Eparvier (1995), On the relationship between the solar soft X ray flux and thermospheric nitric oxide: An update with an improved photoelectron model, J. Geophys. Res., 100, 19,687–19,694.
Solomon, S., D. W. Rusch, J.-C. Gérard, G. C. Reid, and P. J. Crutzen (1981), The effect of particle precipitation events on the neutral and ion chemistry of the middle atmosphere: II. Odd hydrogen, Planet. Space Sci., 8, 885–893.
Solomon, S., G. C. Reid, D. W. Rusch, and R. J. Thomas (1983), Mesospheric ozone depletion during the solar proton event of July 13, 1982: 2. Comparions between theory and measurements, Geophys. Res. Lett., 10, 257–260.
Thomas, L., and M. R. Bowman (1986), A study of pre-sunrise changes in negative ions and electrons in the D-region, J. Atmos. Terr. Phys., 4, 219.
Thomas, R. J., C. A. Barth, G. J. Rottman, D. W. Rusch, G. H. Mount, G. M. Lawrence, R. W. Sanders, G. E. Thomas, and L. E. Clemens (1983), Mesospheric ozone depletion during the solar proton event of July 13, 1982: 1. Measurement, Geophys. Res. Lett., 10, 253–255.
Thomson, N. R., C. J. Rodger, and R. L. Dowden (2004), Ionosphere gives size of greatest solar flare, Geophys. Res. Lett., 31, L06803, doi:10.1029/2003GL019345.
Tobiska, W. K., T. Woods, F. Eparvier, R. Viereck, L. D. B. Floyd, G. Rottman, and O. R. White (2000), The SOLAR2000 empirical solar irradiance model and forecast tool, J. Atmos. Terr. Phys., 62, 1233–1250.
Torr, M. A., D. G. Torr, and R. A. Ong (1979), Ionization frequencies for major thermospheric constituents as a function of solar cycle 21, Geophys. Res. Lett., 6, 771–774.
Turunen, E. (1993), EISCAT incoherent scatter radar observations and model studies of day to twilight variations in the D region during the PCA event of August 1989, J. Atmos. Terr. Phys., 55, 767–781.
Turunen, E., H. Matveinen, J. Tolvanen, and H. Ranta (1996), D-region ion chemistry model, in STEP Handbook of Ionospheric Models, edited by R. W. Schunk, pp. 1–25, SCOSTEP Secretariat, Boulder, Colo.
Ulich, T., E. Turunen, and T. Nygrén (2000), Effective recombination coefficient in the lower ionosphere during bursts of auroral electrons, Adv. Space Res., 25, 47–50.
Vejby-Christensen, L., D. Kella, H. B. Pedersen, and L. H. Andersen (1998), Dissociative recombination of NO^+, Phys. Rev. A, 57, 3627–3634.
Verronen, P. T., E. Turunen, T. Ulich, and E. Kyrölä (2002), Modelling the effects of the October 1989 solar proton event on mesospheric odd nitrogen using a detailed ion and neutral chemistry model, Ann. Geophys., 20, 1967–1976.
World Meteorological Organization (1985), Global ozone research and monitoring project, in Atmospheric Ozone 1985, Rep. 16, Geneva.
Zipf, E. C., P. J. Espy, and C. F. Boyle (1980), The excitation and collisional deactivation of metastable $N(^2P)$ atoms in auroras, J. Geophys. Res., 85, 687–694.

M. A. Clilverd, Physical Sciences Division, British Antarctic Survey, Madingley Road, Cambridge, CB3 0ET, UK.
C.-F. Enell, E. Turunen, and T. Ulich, Sodankylä Geophysical Observatory, Tähteläntie 62, FI-99600 Sodankylä, Finland.
E. Kyrölä, A. Seppälä, and P. T. Verronen, Finnish Meteorological Institute, Earth Observation, P.O. Box 503, FI-00101 Helsinki, Finland. (pekka.verronen@fmi.fi)
C. J. Rodger, Department of Physics, University of Otago, P.O. Box 56, Dunedin, New Zealand.